Self-pulsing and bistability in nonlinear Bragg gratings

Alberto Parini, Gaetano Bellanca, Stefano Trillo, M. Conforti, Andrea Locatelli, Costantino De Angelis

▶ **To cite this version:**

Alberto Parini, Gaetano Bellanca, Stefano Trillo, M. Conforti, Andrea Locatelli, et al.. Self-pulsing and bistability in nonlinear Bragg gratings. Journal of the Optical Society of America B, 2007, 24 (9), pp.2229. 10.1364/JOSAB.24.002229 . hal-02405328

HAL Id: hal-02405328
https://hal.science/hal-02405328

Submitted on 11 Dec 2019

HAL is a multi-disciplinary open access archive for the deposit and dissemination of scientific research documents, whether they are published or not. The documents may come from teaching and research institutions in France or abroad, or from public or private research centers.

L'archive ouverte pluridisciplinaire **HAL**, est destinée au dépôt et à la diffusion de documents scientifiques de niveau recherche, publiés ou non, émanant des établissements d'enseignement et de recherche français ou étrangers, des laboratoires publics ou privés.

Self-pulsing of spatially varying fields in Kerr Bragg gratings

A. Parini, G. Bellanca, S. Trillo
Department of Engineering, University of Ferrara, Via Saragat 1, 44100 Ferrara, Italy

M. Conforti, A. Locatelli, C. De Angelis
Dipartimento di Elettronica per l'Automazione, Università di Brescia, via Branze 38, 25123 Brescia, Italy
(Dated: February 1, 2007)

We present a full characterization of Hopf bifurcations ruling self-pulsing of spatially varying fields in a Bragg grating with Kerr nonlinear response. Our analysis permits, inside the stopband, to distinguish between the fully unstable region and the region where stable high transmission mediated by localized waves is achievable dynamically. Outside the stop-band, it reveals a complex behavior where islands of stability are interspersed between regions of self-pulsing and bistability. Beam propagation simulations validate our linear stability analysis and illustrate the dynamics.

I. INTRODUCTION

Bragg gratings are key elements in several fiber-optics and waveguide applications. The nonlinear response of the costituent materials induces, at high intensities, a whole range of intriguing behaviors that are also characteristics of more complicated nonlinear photonics crystals and spatially periodic structures working at high intensities [1, 2]. In particular when the frequency lies inside (or in the proximity of) one of the bangaps that open up around Bragg resonances, the Bragg grating exhibits different form of competing instabilities encompassing bistability [3] or limiting (frustrated bistability) [4, 5], ordered and disordered self-pulsing (SP) [6–10], modulational instability [11, 12], as well as the possibility of localizing the e.m. field in the form of dispersionless pulses, namely gap solitons [13, 14] (see also Refs. [15, 16] and references therein), which allows for slow-light applications [17] and enable spatial chaos to develop under the action of perturbation that breaks (stationary) integrability [18].

In this work we focus our attention on the temporal stability of generic spatial-dependent stationary solutions in a finite grating, with specific emphasis on the onset of SP and its competition with bistability. The mechanism that underlies SP is the occurrence of a Hopf bifurcation that destabilizes a stationary solution in favour of a stable (in the supercritical case) limit cycle. This is quite common in the nonlinear dynamics of structures that involve feedback either in local form (due to an external mirror or a resonator structure) or distributed (counterpropagating waves coupled linearly or nonlinearly) [19–22]. While SP has been observed in the former case [20, 21], to the best of our knowledge, no clear observations have been reported in purely passive distributed feedback structures with fast nonlinearities structures (preliminar evidence have been reported in Ref. [23] making use of slow nonlinearities). Therefore it is still of paramount importance to characterize the phenomenon theoretically. Previous results based on coupled-mode theory [6–8] as well as FDTD simulations [10] confirm indeed that, in a Bragg grating, SP must be expected in a wide range of parameter values. However, its thorough investigation in the parameter space is still lacking. The aim of this paper is to present a systematic study of SP that allows us to draw a complete stability map, i.e. to determine power and detuning values that lead to the onset of observable SP (versus stable or bistable behaviour) under most common illumination conditions, and to evaluate the frequency of the limit cycle near threshold. Our analysis allows us to establish the region of the gap where localized field solutions (reminiscent of stationary gap solitons) are stable and can be observed by exploiting hysteresis cycles [7], which might necessarily involve, depending on the parameters, spontaneous damping of SP oscillations. For negative out-gap detunings the same stability map reveals an extremely rich behavior where small islands of stability can emerge in between unstable regions. In this region, our approach addresses for the first time the problem of the temporal stability of those stationary evolutions that turn out to be spatially unstable corresponding in phase-space to separatrix crossing [4]. In this case we show that limiting action can be temporally stable for large variations of input power. We validate all the results of the stability analysis with time-dependent simulations of the CMT model and the stationary field pattern by means of transfer matrix approach.

II. THE TIME-DEPENDENT MODEL

We consider a uniform (without any tapering or apodization) Bragg grating or layered dielectric medium characterized by a periodic index modulation $\Delta n(Z)$ with period $\Lambda = 2\pi/\beta_g$ and grating wavenumber β_g. At nonlinear level the medium has a nonlinear Kerr coefficient n_{2I} ($\Delta n = n_{2I} I$, with I the field intensity). Around the m-th order Bragg pulsation ω_{Bm}, the evolution of the forward and backward complex envelopes $u_{\pm}(z,t)$ is governed by the standard non-stationary coupled-mode

equations [15, 16], that we write conveniently in the following dimensionless form

$$-i\left(\frac{\partial u_+}{\partial t}+\frac{\partial u_+}{\partial z}\right)=\delta\beta u_+ +\kappa u_- +\left(|u_+|^2+2\,|u_-|^2\right)u_+,$$
$$-i\left(\frac{\partial u_-}{\partial t}-\frac{\partial u_-}{\partial z}\right)=\delta\beta u_- +\kappa u_+ +\left(|u_-|^2+2\,|u_+|^2\right)u_-, \quad (1)$$

where we define the following normalized detuning and coupling parameters

$$\delta\beta=\left(\beta(\omega)-m\frac{\beta_g}{2}\right)L,\ \ \kappa=\Gamma_m L=k_0\Delta n_p c_m L. \quad (2)$$

where $k_0=2\pi/\lambda_0=\omega/c$, $\beta(\omega)$ is the propagation constant of the mode, $\beta(\omega_{Bm})=m\frac{\beta_g}{2}$, L is the grating length, and we have assumed an index corrugation $\Delta n(Z)=\Delta n_p f(z)$, where $\Delta n_p=n_{max}-n_{min}$ is the peak index contrast and we have assumed that only terms $s=\pm m$ in the Fourier expansion of the periodic function $f(z)=\sum_s c_s\exp(is\beta_g Z)$, $\max|f(z)|=1$, are assumed to be effective (i.e., resonant) in the spirit of the rotating-wave approximation. For instance in a square-wave with 50 % duty cycle, we find at first-order $c_1=1/\pi$, and $\Gamma_1=k_0\Delta n_p/\pi\simeq 2\Delta n_p/\lambda_{B1}$, where $\lambda_{B1}=2\Lambda n_0$ is the first-order Bragg wavelength in vacuum. Positive (negative) detunings correspond to blue(red)-shifted wavelengths with respect to Bragg wavelength, with the stopband (gap) given by $|\delta\beta|<\kappa$.

From the solutions of Eqs. (1) we calculate the total normalized electric field envelope $u=u(z,t)$ as follows

$$u=u_+(z,t)\exp\left(i\frac{\beta_g L}{2}z\right)+u_-(z,t)\exp\left(-i\frac{\beta_g L}{2}z\right). \quad (3)$$

Though the use of dimensionless quantities is convenient for the following analysis, it is useful to recall the link with real-world variables: $z=Z/L$ and $t=T/T_s$ are distance and time in units of grating length L and transit time $T_s=L/V_{gm}$, where $V_{gm}=d\beta/d\omega^{-1}\simeq c/n_0$ is the group-velocity calculated at m-th order Bragg frequency. Furthermore the real-world powers of the counterpropagating beams as well as the total power are given by $\gamma L|u_\pm|^2$ and $\gamma L|u|^2$, respectively, where $\gamma=k_0 n_{2I}/A_{eff}$ is the overall nonlinear coefficient in [m^{-1} W^{-1}], A_{eff} being the effective area of the mode (for plane waves in a bulk layered medium [24], $\gamma=k_0 n_{2I}$, and $\gamma L|u|^2$ or $\gamma L|u_\pm|^2$ are intensities). Although we consider only focusing nonlinearities inducing a red-shift of the stopband, the conclusions of the paper hold true also for defocusing nonlinearities when the sign of the detuning is reversed ($\delta\beta\to-\delta\beta$).

Stationary solutions of Eqs. (1) describe the spatial evolution of the two interacting fields in the interval $z=[0,z_L=1]$, subject to general boundary conditions (note that the absolute phase of $u_+(z=0)$ can be set to zero without loss of generality due to invariance of Eqs. (1) under the transformation $u_\pm\to u_\pm\exp(i\psi)$)

$$u_+(z=0)=\sqrt{P_{in}^+}\ ;\ ,u_-(z_L=1)=\sqrt{P_{in}^-}\exp(i\phi_0), \quad (4)$$

Eqs. (1) with $\partial/\partial t=0$ constitute a well-defined ODE boundary value problem, which can be solved numerically. by means of, e.g. shooting method.

III. THE LINEAR STABILITY ANALYSIS

In the non-stationary case, time-dependent perturbations can grow on top of the (stationary) spatially varying fields, thus destabilizing the device. A typical scenario, in systems with feedback, involves the occurence of a Hopf bifurcation which is responsible for SP. The latter can be characterized by standard stability analysis starting from perturbed steady-state solutions of the kind

$$u_\pm(z,t)=a_\pm(z)+p_\pm(z,t), \quad (5)$$

where the stationary solutions $a_\pm$ obey Eqs. (1) with $\partial_t=0$, or explicitly

$$\mp i\frac{\partial a_\pm}{\partial z}=\delta\beta\ a_\pm+\kappa a_\mp+\left(|a_\pm|^2+2\,|a_\mp|^2\right)a_\pm, \quad (6)$$

whereas the perturbations $p_\pm$ obey the following linearized system, obtained by inserting Eq. (5) in Eqs. (1), and dropping nonlinear terms in $p_\pm$ (in the standard hypothesis $|p_\pm|\ll|a_\pm|$)

$$\frac{\partial p_\pm}{\partial t}+\frac{\partial p_\pm}{\partial z}=i\delta\beta p_\pm+i\kappa p_\mp+i\left(a_\pm^2 p_\pm+2|a_\pm|^2 p_\pm\right)+2i\left(a_\mp a_\pm^* p_\pm+a_\mp a_\pm p_\mp^*+a_\mp^* a_\pm p_\mp\right). \quad (7)$$

Even if Eqs. (7) are linear, they are still partial differential equations and stability properties cannot be easily assessed. However, following the approach outlined in Ref. [22], we reduce them to N ordinary differential equations (ODEs) by discretizing the interval $[0,z_L]$ with N equally spaced points, obtaining a uniform grid z_j, $j=1,\ldots,N$, with step-size $h=\frac{z_L}{N-1}$. By doing so, and by splitting complex quantities into real/imaginary parts as $p_\pm=p_\pm^r+ip_\pm^i$ and $a_\pm=a_\pm^r+ia_\pm^i$ and finally approximating spatial derivatives with finite differences, we cast Eqs. (7) in the following form

$$\dot p(t)=M\ p(t), \quad (8)$$

where the dot stand for d/dt, $M=M\left[P_{in}^\pm,\phi_0,\delta\beta,\kappa\right]$ is a $4N\times 4N$ matrix that depends on both the parameters and stationary boundary values (see Appendix A), and the real perturbation $4N$ vector is $p(t)=\left[p_+^r(t),p_+^i(t),p_-^r(t),p_-^i(t)\right]^T$ with $p_\pm^{r,i}(t)=\left[p_\pm^{r,i}(z_1,t),\ldots,p_\pm^{r,i}(z_N,t)\right]^T$.

Instability occurs when one (or more) eigenvalue of

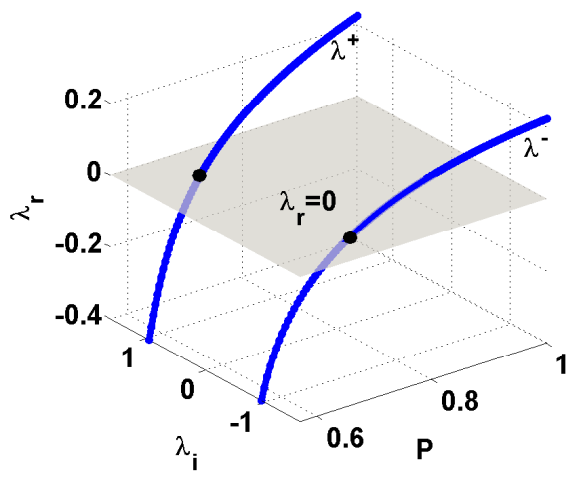

Figure 1: Hopf bifurcation: the leading pair of complex conjugate eigenvalues $\lambda^{\pm} = \lambda_r \pm i\lambda_i$ crosses the plane $\lambda_r = 0$ as the control parameter P is increased. Here $\delta\beta = 1.5$ and $\kappa = 2.5$.

the matrix M crosses the imaginary axis entering the right-half complex plane, thereby entailing exponential growth of the perturbation. A Hopf bifurcation occurs whenever a pair of complex conjugate eigenvalues $\lambda^{\pm} = \lambda_r \pm i\lambda_i$ cross into the right-half plane $\lambda_r > 0$. This corresponds to the stationary solution undergoing SP or self-oscillation with (normalized) temporal period

$$t_{SP} = \frac{2\pi}{\lambda_i}, \tag{9}$$

above the marginal condition (instability threshold) determined by the condition $\lambda_r = 0$.

In principle the onset of SP can be characterized by studying the bifurcations of Eq. (8), i.e. how eigenvalues move in the five dimensional parameter space $P, P_-, \phi_0, \delta\beta, \kappa$. Although we find that, with external parameters $\delta\beta, \kappa$ fixed, the Hopf bifurcation occurs under general illumination conditions ($P_{in}^{\pm}, \phi_0 \neq 0$), its observability in a real experiment would require a coherent control of the relative phase of counterpropagating beams, which introduces inessential complication. Viceversa the simplest experimental arrangement involves unidirectional illumination, i.e. $P_{in}^{-} = 0$ for which the dynamics is phase-insensitive (ϕ_0 plays no longer any role). Therefore, in view of discussing the most favourable conditions, we restrict ourselves to discuss this case.

IV. RESULTS (UNI-DIRECTIONAL ILLUMINATION)

In the case of uni-directional forward illumination, the evolutions depends only on two external parameters,

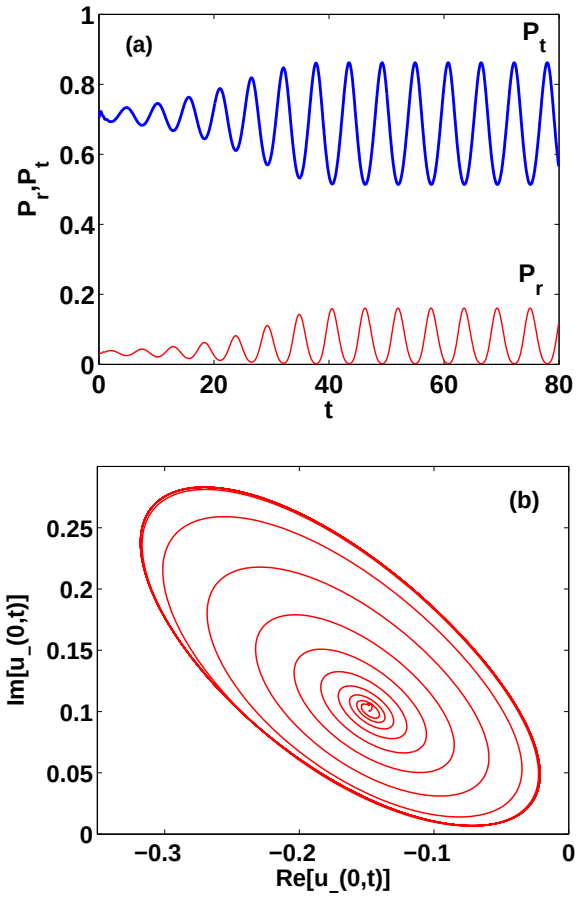

Figure 2: (a) Temporal evolution of transmitted (P_t) and reflected (P_r) powers of a SP-unstable solution, for $\delta\beta = 1$, $\kappa = 2.5$, $P = 0.7$); (b) phase-space portrait.

namely $\delta\beta, \kappa$, and input power $P_{in}^{+} = P_{in}$ (we drop superscript + henceforth). However, because of bistability, neither the transmission nor the reflection are single-value functions of P_{in}. Therefore it is more convenient to use as a parameter the power flux

$$P = |a_+(z)|^2 - |a_-(z)|^2, \tag{10}$$

which is a steady-state invariant of Eqs. (6). In the case of uni-directional illumination $|a_-(z_L)|^2 = 0$ and so $P = |a_+(z_L)|^2$ represents the steady-state transmitted power. By tracking the leading (largest real part) eigenvalues of Eq. 8 against variation of P (with fixed κ and $\delta\beta$), our algorithm yields a clear picture of the Hopf bifurcation, as exemplified in Fig. 1 for $\delta\beta = 1$, $\kappa = 2.5$: in this case a leading pair of complex conjugate eigenvalues bifurcate at $P = P_{Hopf} \simeq 0.8$. The result of the linear stability analysis can be checked by integrating numerically Eqs. (1) and looking at measurable quantities, namely the temporal behavior of transmitted power $P_t = |u_+(0,t)|^2$ and reflected power $P_r = |u_-(0,t)|^2$. Slightly above the threshold predicted by the stability analysis we find that transmitted and reflected powers

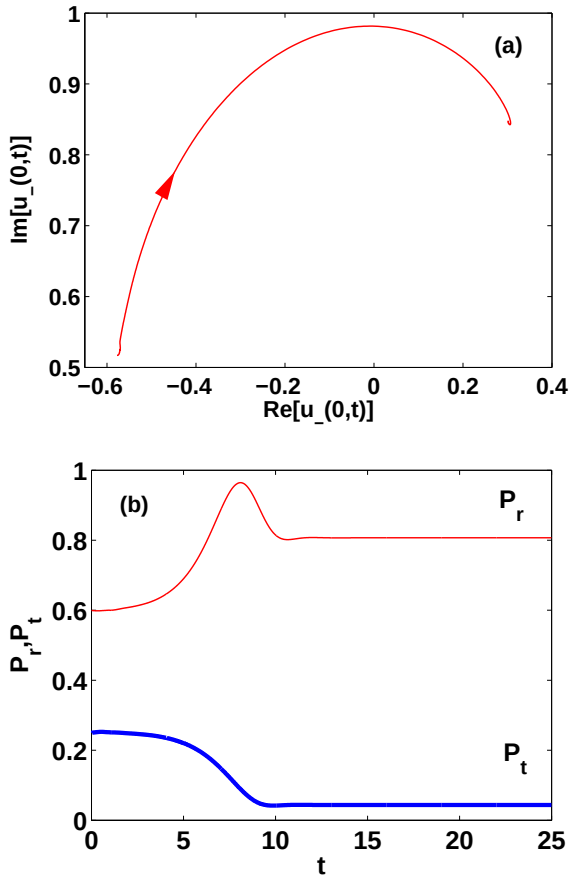

Figure 3: (a) Phase space evolution for initial conditions sitting on the negative slope branch of the bistable response (here $\delta\beta = 1$, $\kappa = 2.5$, $P = 0.25$). (b) Corresponding temporal evolutions of transmitted and reflected powers.

exhibit regular out of phase oscillations as shown in Fig. 2(a). Fourier transforming these temporal series we obtain a normalized period $t_{SP} = 5.7$ (i.e., $5.7T_s$ in real-world units) in good agreement with the linear estimate $2\pi/\lambda_i = 5.6$. Close to the bifurcation point we always find the representative point of the nonlinear mixing to evolve, after a short transient, along a limit cycle [see Fig. 2(b)], thus proving the supercritical character of the bifurcation. We find that, only far from threshold, the limit cycle destabilizes [6, 7] leading eventually to temporal chaos, a regime that we will not consider any further here.

However, for given values of the parameters, our linearized system (8) yields also real positive eigenvalues. This is found to be always the case when the steady-state lies on the negative-slope branch of the bistable response. In this case the system destabilizes without undergoing to self-oscillation. As illustrated in the example of Fig. 3 corresponding to $\delta\beta = 1$, $\kappa = 2.5$, $P = 0.25$, the system evolves asymptotically towards a new steady-state characterized by different spatial profiles of the fields. In this case the final status is found to be on the (stable) lower

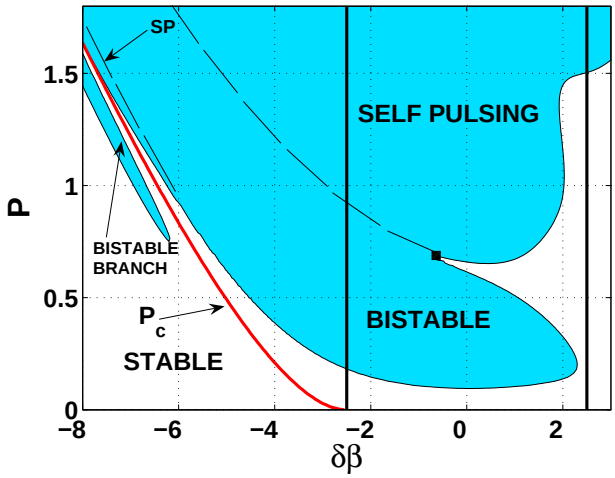

Figure 4: Stability map in the parameter plane $\delta\beta - P$ (detuning - transmitted power), for $\kappa = 2.5$ (gap edges $\delta\beta = \pm 2.5$ shown as vertical lines). The white and hatched areas correspond to temporally stable and unstable regions, respectively. Merging of bistable and SP domains occuring at critical detuning $\delta\beta_c$ is highlighted by a square mark. The curve $P = P_c(\delta\beta)$ (solid, red) gives basically the level of the transmission plateau for negative out-gap detunings (see text).

branch of the bistable response.

We are able to discriminate between temporally stable behaviors and the two aforementioned competing mechanisms of instability by drawing a map of the leading eigenvalues in the control parameter plane $\delta\beta - P$, with fixed coupling coefficient κ. A typical result obtained for $\kappa = 2.5$ (other values of the coupling parameter give qualitatively similar results) is shown in Fig. 4. In the following we discuss separately the three regions corresponding to in-gap ($|\delta\beta| < \kappa$) and positive or negative out-gap detunings.

A. In-gap detuning

For detunings within the gap ($|\delta\beta| < \kappa$), the linear stability analysis yields a region of stability (all eigenvalues have negative real part) at low values of P, followed by a region of real unstable eigenvalues (intermediate values of P), and a region of SP (complex conjugate eigenvalues, large values of P). Importantly, our analysis shows that there is a critical value of detuning ($\delta\beta_c \sim -0.4$ in Fig. 4, highlighted by a square) below which the domain of bistability and SP merge. In this regime, i.e. for $\delta\beta < \delta\beta_c$, only the lower branch of the bistable response is temporally stable, and no stable dynamics or nonlinear switching to the upper branch (including transparency) can ever be observed.

Interestingly enough, however, for positive detunings a window of stability appears, separating bistability from SP domains. This means that a portion of the upper

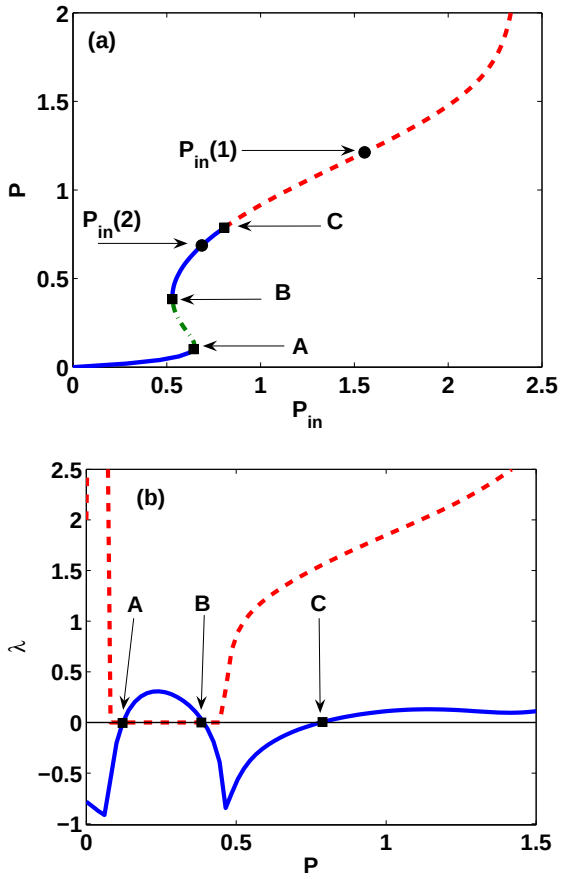

Figure 5: (a) Steady-state input-output characteristic P vs. P_{in} for grating parameters $\delta\beta = 1.75$ and $\kappa = 2.5$. The solid line indicates stable portions, whereas unstable portions are dashed (SP, complex conjugate eigenvalues), or dot-dashed (bistability, real eigenvalues). (b) Real (solid line) and imaginary (dashed line) part of the leading eigenvalues vs. P. Points A,B,C denote bifurcation points where eigenvalues with positive real parts appear (A,C) or disappear (B). $P_{in}(1,2)$ are excitation levels employed in the simulations of Fig. 6.

branch with positive slope turns out to be stable, as illustrated in the steady state response reported in Fig. 5(a). The results of the linear stability analysis, shown in Fig. 5(b), indicate that the two knees (points A and B) of the response have one to one correspondence with the bifurcation points where the leading real eigenvalue appears and disappears, respectively. The stable portion of the response corresponds to values of P in between the points B and C, where all eigenvalues have negative real part. The point C denotes the Hopf bifurcation point above which SP is expected (at threshold $t_{SP} \sim 4$).

When the window of stability includes the transparency point on the upper branch of the steady-state (i.e., $P = P_{in}$), a localized field reminiscent of a gap soliton can be excited dynamically by exploiting hysteresis and spontaneous damping of SP oscillations that occurs when the device is driven with $P_{in} > P_{in}(C)$. An example of the underlying temporal dynamics is reported in Fig. 6. We first raise the input power by following the simple exponential law shown by the dashed curve in Fig. 6(a) up to the level $P_{in} = P_{in}(1)$ lying on the upper branch above the Hopf bifurcation point C [see in Fig. 5(a)]. The input power is initially strongly reflected, until P_{in} reaches the first knee (point A) causing the reflected power to drop and the transmitted power to increase abruptly. However, immediately after the switching point the onset of SP makes stable high-amplitude oscillations visible in both reflection [Fig. 6(a)] and transmission [Fig. 6(b)]. From this regime, we stabilize the system on the upper branch by decreasing P_{in} up to the transparency level $P_{in}(2)$. In fact, when crossing the bifurcation point C, both the reflected and tramsmitted powers settle down to steady-state levels, while the field is strongly localized (as a strict gap soliton, except for the tails that do not tend asymptotically to zero), as shown in Fig. 6(c). Decreasing further P_{in} up to the knee point B, the field remains stable and localized, though in a less transmissive state. Decreasing further P_{in} leads to down-switching (not shown). We point out that, when working closer to the critical detuning $\delta\beta_c$, the stable portion of the upper branch shrinks until its location stands entirely on the left of the knee point A. In this case up-switching involves *necessarily* SP regardless of the input power level used to drive the up-switching. Moreover, our analysis permits to conclude that fields with stronger properties of localization which are obtained when operating close to the red edge of the gap, cannot be observed because the device is fully unstable.

B. Positive out-gap detunings

This is the least interesting region because the linear transmissive behavior of the grating is marginally altered by the nonlinear response, which tends to detune further the structure from resonance. As a consequence, bistability disappears, and SP occurs only at very large values of P, in turn requiring very high input powers.

C. Negative out-gap detunings

The region of large (out-gap) negative detunings is interesting because our intuition tells us that, at sufficiently high power (the larger the detuning, the higher the power), the red-shift of the stopband can alter linear transmissive properties, making the device reflective (somehow the opposite of what happens when operating inside the stopband). Although this picture is basically correct, the nonlinear switching to the reflective state is less simple than that and turns out to be mediated by the occurence of *spatial instabilities*. While we present a detailed discussion of the latter phenomenon in terms of phase-space analysis in Appendix B, here it is sufficient to

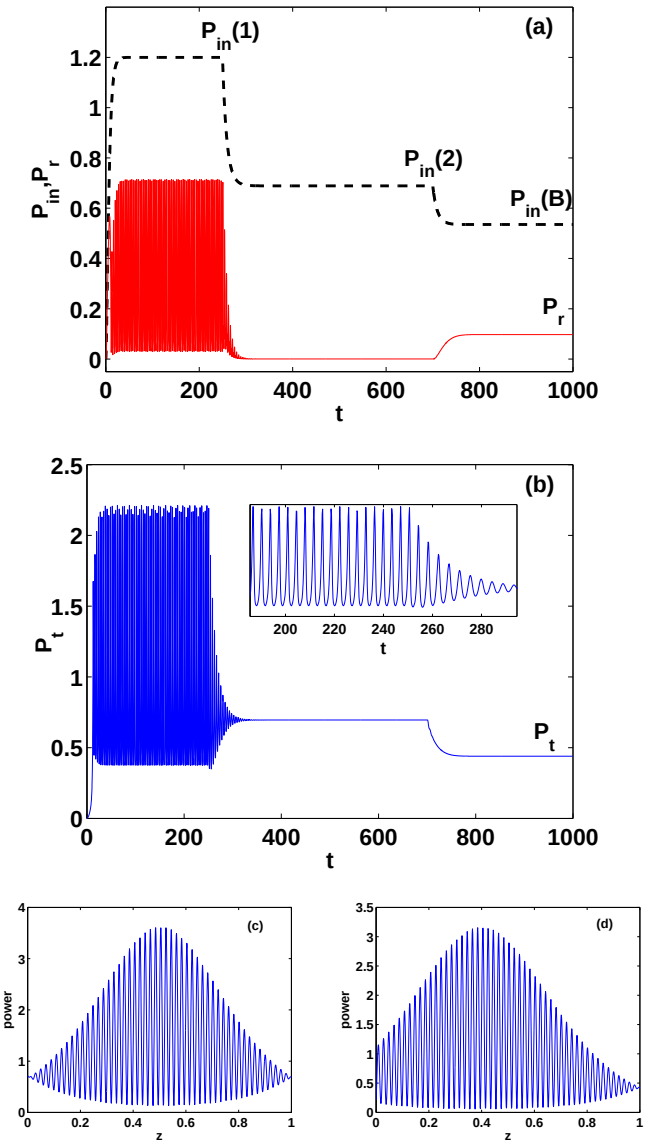

Figure 6: (a) Transmitted power $P_t(t)$ vs. time t (solid line) in response to the excitation $P_{in}(t)$ (dashed line); (b) Reflected power $P_r(t)$, with inset showing a detail of the damped oscillations; (c-d) Spatial profiles of the total power $|u(z)|^2$ after reaching steady-state at transparency point [(c), $t = 600$] and at knee point B [(d), $t = 1000$] Parameters are as in Fig. 5.

recall briefly how spatial instabilities affect the behavior of the device. Since the detuning is out-gap, for relatively low input powers the device is substantially transparent and the fields experience small spatial oscillations. In this regime, only tiny bistability cycles can take place caused by fact that the spatial period of the small oscillations increases with power. However, when the input power reaches a critical value (corresponding to a given critical value of output power $P = P_c$), the period tends to infinity and the evolution becomes asymptotic. Very large increase of input power above this value results in very small changes of transmitted power above the value P_c, the power being mainly reflected. Therefore the output power remains nearly clamped to a transmitted plateau $P \sim P_c$ and the device acts as a limiter in transmission, as shown by the typical input-output response reported in Fig. 7(a). While the extension of the plateau depends on the coupling strength (it extends to higher input powers with κ increasing) the clamping power P_c depends only on the detuning (see Appendix B for its calculation). Importantly, we find that the curve $P_c = P_c(\delta\beta)$ falls in the temporally stable region of the stability map in Fig. 4. The map suggests indeed that, for relatively small detunings ($|\delta\beta| < 6$), the transmission plateau (which corresponds to P slightly above P_c, in turn corresponding to large increase of input powers) is entirely contained in the stable region, and hence limiting action is temporally stable and hence fully observable. The system destabilizes only at values of P entering the bistable domain in Fig. 4 in turn correponding to the wide negative slope branch of the bistable response in Fig. 7(a). Finally, the higher branches with positive slope are found to be all SP unstable. Conversely, the situation is more intriguing for large detunings ($|\delta\beta| > 6$), because the curve $P_c = P_c(\delta\beta)$ is still in the stable region, but interspersed between a small island of bistability and a tiny portion (labeled SP in Fig. 4) embedded in the fully unstable region. While the island can be understood to correspond to the negative slope branch of the small bistable cycle that precedes the plateau in Fig. 7(a), temporal stability on the endmost portion of the transmission plateau [dashed part in Fig. 7(a)] is lost via SP, owing to the tiny region that precedes the large bistable domain in Fig. 4.

These results are validated by integration of Eqs. (1). Fig. 7(b) shows the temporal evolution of transmitted and reflected powers when the input power is raised monotonically up to the peak level $P_{in}(1)$ right below the onset of SP. As shown the curves reach the steady-state in a quasi-mononotonic way (small features at early times $t \simeq 20$ are due to the small bistability cycle present in the transparent region, and discussed above]. Viceversa, when the peak is set to $P_{in}(2)$ slightly above threshold, the system clearly exhibits large-scale temporal oscillations characteristic of SP.

Finally, one can naturally wonder whether the spatial instabilities and the underlying dynamics can be an artifact of the coupled-mode theory, whose validity is known to be limited to shallow and weakly nonlinear gratings. In order to show that this is not so, we have employed the transfer matrix method (TMM) [10, 26, 27]. Even considering an index contrast as high as $\Delta n_p = 0.2$ (all other parameters are such to give the same normalized parameters of the couped-mode theory), the steady-state response given by the latter method shows a transmissive plateau, which presents only a small quantitative discrepancy, mainly in terms of estimating the clamping power P_c, with the result of the coupled-mode theory (see Fig. 8). This descrepancy vanishes in the limit of shallow gratings.

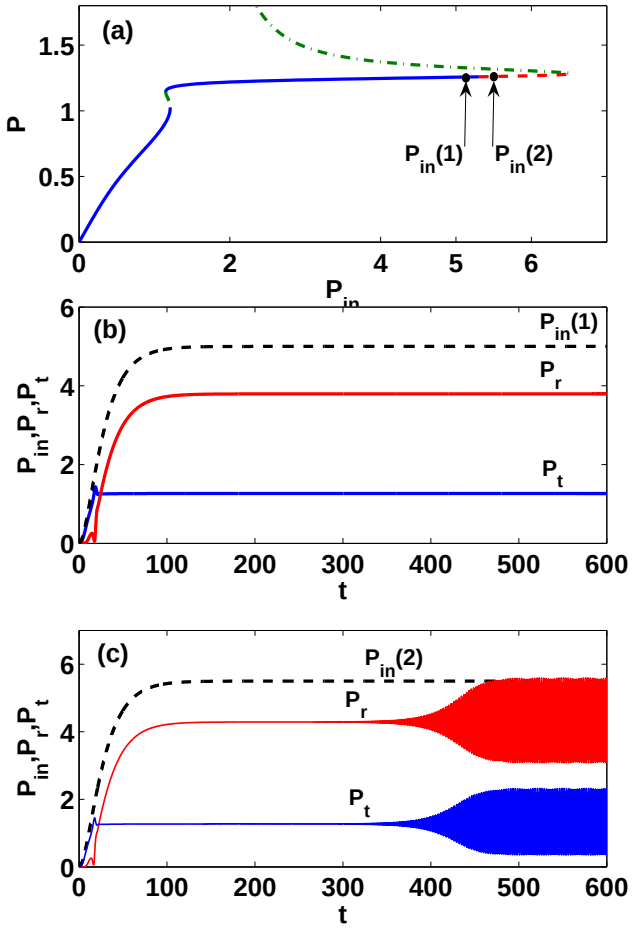

Figure 7: (a) Steady-state transmission characteristic: P vs. P_{in} for $\delta\beta = -7$, $\kappa = 2.5$. (b) Stable temporal evolution of P_t and P_r corresponding to an input power raised monotonically up to the value $P_{in}(1)$ in the stable domain. (c) Onset of SP when the input power is raised up to the value $P_{in}(2)$ in the unstable domain.

V. CONCLUSIONS

In summary, we have presented a systematic analysis of SP instabilities in a Bragg grating. We have found that, inside the stopband, the upper branch of the bistable response can be partially stable above a critical detuning. When the stable portion includes the transparency point, localized fields reminescent of gap solitons can be stably excited by means of hysteresis cycles that might involve spontaneous damping of SP oscillations. We have also assessed the temporal stability of the large transmission plateau (limiting caused by the onset of spatial instabilities) in the region of out-gap negative detunings.

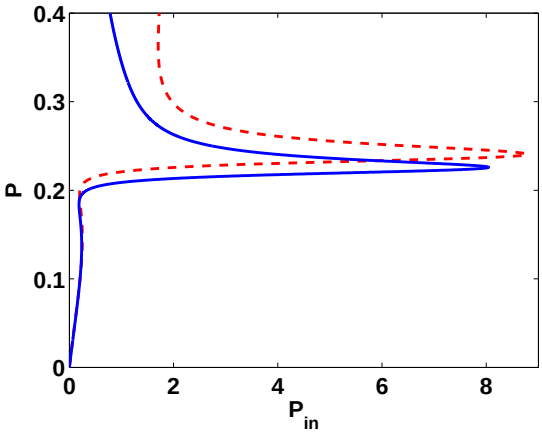

Figure 8: Steady-state transmission characteristic: coupled-mode theory (solid blue) against transfer matrix method (dashed red). The transfer matrix results is obtained for grating parameters $\Lambda = 250nm$, $n_0 = 2$, $\Delta n_p = 0.2$, $n_{2I} = 10^{-20}$ m^2/W, and all other parameters such to fit the normalized parameters ($\delta\beta = -7$, $\kappa = 5$) and powers used in Eq. (1).

VI. APPENDIX A: TEMPORAL STABILITY PROBLEM

The matrix of the linearized system (8) has the structure of a 4×4 matrix $M = \{M_{ij}\}$, $i, j = 1, 2, 3, 4$, where the single blocks M_{ij} are in turn $N \times N$ matrices of the following form

$$
\begin{aligned}
M_{11} &= -A_B - 2R_+I_+; \\
M_{12} &= -\delta\beta I_N - R_+^2 - 3I_+^2 - 2R_-^2 - 2I_-^2; \\
M_{13} &= -4R_-I_+; \\
M_{14} &= -\kappa I_N - 4I_-I_+; \\
M_{21} &= \delta\beta I_N - 2R_-^2 + 2I_-^2 + I_+^2 + 3R_+^2; \\
M_{22} &= -A_B + 2R_+I_+; \\
M_{23} &= \kappa I_N + 4R_-R_+; \\
M_{24} &= 4I_-R_+; \\
M_{31} &= -4R_+I_-; \\
M_{32} &= -\kappa I_N - 4I_+I_-; \\
M_{33} &= A_F - 2I_-R_-; \\
M_{34} &= -\delta\beta I_N - R_-^2 - 3I_-^2 - 2R_+^2; \\
M_{41} &= \kappa I_N - 4R_+R_-; \\
M_{42} &= 4I_+R_-; \\
M_{43} &= \delta\beta I_N + I_-^2 + 2R_+^2 + 2I_+^2 + 3R_-^2; \\
M_{44} &= A_F + 2I_-R_-.
\end{aligned}
\tag{11}
$$

Here A_F [which has nonvanishing elements $A_F(j,j) = 1/h$, $j = 1, \ldots, N$ and $A_F(j, j-1) = -1/h$, $j = 2, \ldots, N$], and A_B [which has nonvanishing elements $A_B(j,j) = -1/h$, $j = 1, \ldots, N$ and $A_B(j-1, j) = 1/h$, $j = 2, \ldots, N$] stand for forward and backward finite-differences matrices, respectively, $R_\pm\,(I_\pm)$, are $N \times N$ diagonal matrices whose elements consist of the real

(imaginary) parts of the stationary solutions $a_\pm$ evaluated at the grid points z_j [i.e., $R_\pm(j,j) = a^r_\pm(z_j)$, $I_\pm(j,j) = a^i_\pm(z_j)$], while I_N is the unit matrix.

VII. APPENDIX B: STEADY-STATE SPATIAL INSTABILITIES

In this appendix we discuss bifurcations and spatial instabilities of the stationary model [Eqs. (6)] originating from the existence unstable eigenmodes, i.e. particular combinations of forward and backward phase-locked waves that correspond to saddle point in phase space. The analysis can be conveniently carried out by exploiting the conservative structure of Eqs. (6) cast in the form

$$\mp i\frac{da_\pm}{dz} = \frac{\partial H}{\partial a^*_\pm}, \tag{12}$$

where the z-invariant Hamiltonian is $H = \delta\beta\left(|a_+|^2 + |a_-|^2\right) + \kappa\left(a_+a^*_- + a_-a^*_+\right) + \left(|a_+|^4/2 + |a_-|^4/2 + 2|a_+a_-|^2\right)$. The Hamiltonian structure, together with Poynting conservation $|a_+|^2 - |a_-|^2 = P$, can be easily exploited as follows. First, by expressing the complex amplitudes in terms of intensity and phase as $a_- = \sqrt{\eta}\exp(i\phi_-)$, $a_+ = \sqrt{P+\eta}\exp(i\phi_+)$ we obtain, by direct substitution in H or equivalently in Eqs. (6), the following reduced system of two real equations

$$\frac{d\eta}{dz} = -\frac{\partial H_r}{\partial\phi} \;\; ; \;\; \frac{d\phi}{dz} = \frac{\partial H_r}{\partial\eta}, \tag{13}$$

$$H_r = 2\delta\beta\;\eta + 2\kappa\sqrt{\eta(\eta+P)}\cos\phi + 3\eta(\eta+P) \tag{14}$$

where $\phi = \phi_+ - \phi_-$ is the effective phase, and $H_r = H_r(\eta,\phi)$ is the reduced Hamiltonian, whose (constant) value of interest is constrained by the boundary condition $\eta_L = \eta(z_L) = 0$ to be $H_r = H_r(\eta_L,\phi) = 0$. The latter condition allows us to express the first of Eqs. (13) as a self-consistent equation in η only [eliminating ϕ in the RHS of the equation by means of Eq. (14)], which can be integrated in the backward direction to obtain the solution for $\eta(z) \equiv |a_-(z)|^2$ in terms of the following quadrature integral

$$z - z_L = \int_0^{\eta(z)} \frac{d\eta}{\sqrt{f(\eta)}}, \tag{15}$$

where $f(\eta) = 4\eta(P+\eta) - \eta^2[2\delta\beta + 3(1+\eta)]^2$. Knowing $\eta(z) = |a_-(z)|^2$ one obtains also $|a_+(z)|^2 = P+\eta(z)$. Explicit form of the solutions can be obtained by inverting the integral (15) in terms of Jacobian elliptic functions [3, 4].

Eigenmodes $\eta = \eta_e$, $\phi = \phi_e$ correspond to equilibrium points of Eqs. (14), and follow the bifurcation structure shown in Fig. 9. As shown in Fig. 9a, at $P = 0$, the system presents two transcritical bifurcations where

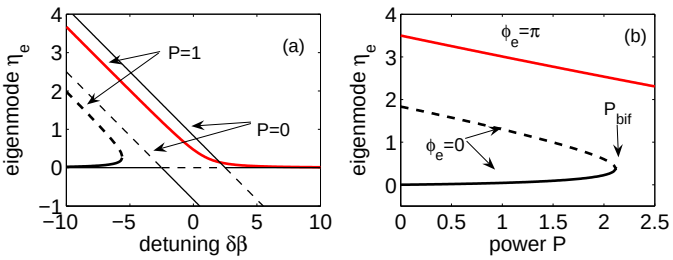

Figure 9: Bifurcation structure ($\kappa = 2.5$): equilibrium points η_e as a function of (a) detuning $\delta\beta$ for $P = 0$ (thin lines) and $P = 1$ (thick lines); (b) power P for a fixed detuning $\delta\beta = -8$. Solid and dashed lines stand for stable points (centers) and unstable points (saddles), respectively. Physical solutions are those contained in the semi-plane $\eta_e \geq 0$ (η_e is a power).

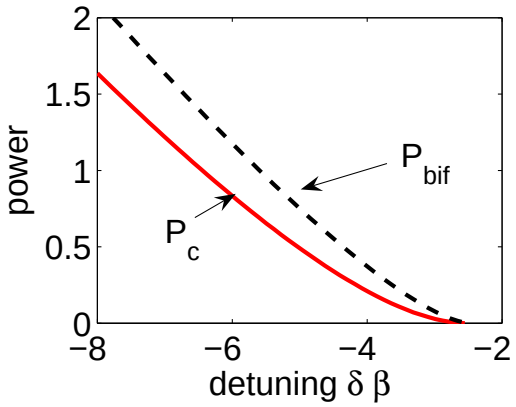

Figure 10: Bifurcation and clamping powers P_{bif}, P_c (see text for their definition) vs. detuning $\delta\beta$ ($\kappa = 2.5$).

two branches of phase-locked eigenmodes $\phi_e = \frac{\pi}{2} \pm \frac{\pi}{2}$, $\eta_e = (\delta\beta \mp \kappa)/3$, exchange stability with the eigensolution $\eta_e = 0$ exactly at the gap edges (bifurcation points $\delta\beta = \pm\kappa$). Incidentally the separatrices that emanate from the origin ($\eta_e = 0$) and from the phase-locked saddle point $\phi_e = 0$, $\eta_e = (\delta\beta + \kappa)/3$ correspond to stationary (zero velocity) bright in-gap solitons and dark-antidark out-gap soliton pairs, respectively, as discussed thoroughly in Ref. [16]. As well known, however, bright still solitons are not accessible physically because they corresponds to zero field on both boundaries, whereas dark-antidark pairs cannot be excited with zero backward illumination. Nevertheless a deformation of the latter type of separatrices affect the dynamics deeply for $P \neq 0$ (implying non-zero transmitted power). In this case the bifurcation diagram turns out to be a deformation of the one at $P = 0$, in which the transcritical bifurcation occuring at $\delta\beta = -\kappa$ becomes a saddle-center [see Fig. 9(a)], while the one at $\delta\beta = \kappa$ disappears leaving an isolated stable branch. Importantly, the saddle-center feature appears also by drawing the diagram against power P at fixed (negative and out-gap) detunings, as shown in Fig. 9(b). In this case, the saddle-center pair exists for

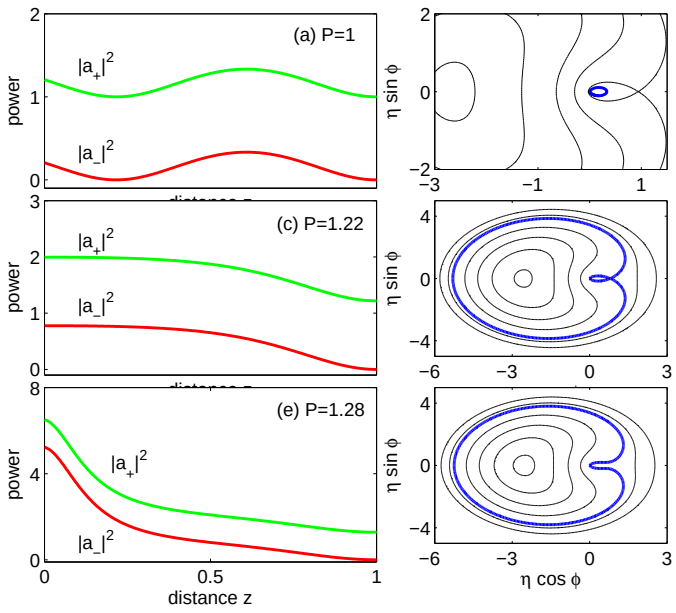

Figure 11: Spatial evolution of the field intensities for $\delta\beta = -7$, $\kappa = 2.5$, and different values of P. The right frames show the corresponding phase-space pictures, with the followed trajectory reported in bold.

$P < P_{bif}$, where the bifurcation power P_{bif} is a function of the detuning as shown explicitly in Fig. 10. In particular, the existence of a saddle $P < P_{bif}$ implies that small changes of initial conditions or parameters can lead to cross the separatrix that emanates from the saddle point, thus leading to qualitatively different behaviors. In the case of interest here, separatrix-crossing occurs by changing P at fixed $\delta\beta$ and leads to limiting action in transmission, as first discussed in Ref. [4] (see also Ref. [18, 25]). The underlying dynamics is illustrated in Fig. 11: trajectories emanating from the point $\eta = \eta(z_L) = 0$ can be of the weak-coupling type (small oscillations, for small values of power $P < P_c$) or strong-coupling case (large values of powers $P > P_c$). In the latter regime, tiny changes of output powers P above P_c give rise to large increase of input powers, or reversing the argument, large changes of input power produces tiny changes of output power and hence limiting action. The critical value of output power $P = P_c$ that discriminates between the two regimes corresponds to a separatrix evolution on which, going in the backward direction, the intensity evolutions proceed asymptotically from their output values towards the constant value corresponding to the saddle point. Basically the output power remains clamped to $P \simeq P_c$ for large changes of input power. At fixed detuning, the value P_c can be calculated by imposing the constraint $H(\eta = 0) = H(\eta_e, \phi_e | P_c)$, arising from the conservation of the Hamiltonian between the point $\eta(z_L) = 0$ and the saddle $\eta = \eta_e, \phi_e = 0$ corresponding to the value of the parameter $P = P_c$. The outcome of this calculation as a function of the detuning is reported in Fig. 10.

[1] R.E. Slusher and B.J. Eggleton, eds. *Nonlinear Photonics Crystals* (Springer-Verlag, Berlin, 2003).

[2] C. M. Bowden and A. M. Zheltikov, Eds., *Nonlinear Optics in Photonics Crystals*, Feature issue, J. Opt. Soc. Am. B (2002).

[3] H.G. Winful, J.H. Marburger, and E. Garmire, "Theory of bistability in nonlinear distributed feedback structures", Appl. Phys. Lett. **35**, 379-381 (1979).

[4] A. Mecozzi, S. Trillo, and S. Wabnitz, "Spatial instability, all-optical limiting and thresholding in nonlinear distributed feedback devices", Opt. Lett. **12,** 1008-1010 (1987).

[5] C. J. Herbert, W. S. Capinski, and M. S. Malcuit, "Optical power limiting with nonlinear periodic structures", Opt. Lett. **17**, 1037-1039 (1992).

[6] H.G. Winful, G.D. Cooperman, "Self-pulsing and chaos in distributed feedback bistable optical devices", Appl. Phys. Lett. **40**, 298-300 (1982).

[7] C.M. de Sterke and J. Sipe, "Switching dynamics of finite periodic nonlinear media: a numerical study", Phys Rev. A **42** 2858-2869 (1990).

[8] C. M. de Sterke, "Stability analysis of nonlinear periodic media", Phys. Rev. A 45, 82528258 (1992).

[9] A.B. Aceves, S. Wabnitz, C. De Angelis, "Generation of solitons in a nonlinear periodic medium", Opt. Lett. **17**, 1566-1568 (1992).

[10] A. Parini, G. Bellanca, S. Trillo, L. Saccomandi, P. Bassi, "Transfer matrix and full Maxwell time domain analysis of nonlinear gratings", Opt. Quantum Electronics **36**, 189-199 (2004).

[11] C. M. de Sterke, "Theory of modulational instability in fiber Bragg gratings", J. Opt. Soc. Am. B **15**, 2660-2667 (1998).

[12] S. Pitois, M. Haelterman, and G. Millot, "Theoretical and experimental study of Bragg modulational instability in a dynamic fiber grating", J. Opt. Soc. Am. B **19**, 782 (2002).

[13] W. Chen and D. L. Mills, "Gap solitons and the nonlinear optical response of superlattices", Phys. Rev. Lett. **58**, 160-163 (1987).

[14] B. J. Eggleton, R. E. Slusher, C. M. de Sterke, P. A. Krug, and J. E. Sipe, "Bragg grating solitons", Phys. Rev. Lett. **76**, 1627-1630 (1996).

[15] M. de Sterke, B. Eggleton, and J. Sipe, in *Spatial Solitons*, S. Trillo and W.E. Torruellas, eds., (Springer, Berlin, 2001).

[16] C. Conti and S. Trillo, "Bifurcation of gap solitons through catastrophe theory", Phys. Rev. E **64**, 036617 (2001).

[17] J. T. Mok, C. M. De Sterke, I. C. M. Littler, and B. J. Eggleton, "Dispersionless slow light using gap solitons", Nature Phys. **2**, 775-780 (2006).

[18] S. Trillo, C. Conti, G. Assanto, A. V. Buryak, "From parametric gap solitons to chaos by means of second-

harmonic generation in Bragg gratings", Chaos **10**, 590-600 (2000).

[19] Y. Silberberg and I. Bar-Joseph, "Instabilities, self-oscillation and chaos in a simple nonlinear optical interaction" Phys. Rev. Lett. 48, 15411544 (1982).

[20] C. Richy, K. I. Petsas, E. Giacobino, C. Fabre, and L. Lugiato, "Observation of bistability and delayed bifurcation in a triply resonant optical parametric oscillator, J. Opt. Soc. Am. B 12, 456461 (1995).

[21] M. Bache, P. Lodhal, A. V. Mamaev, M. Marcus, and M. Saffman, "Observation of self-pulsing in singly resonant optical second-harmonic generation with competing nonlinearities, Phys. Rev. A **65**, 033811 (2002).

[22] M. Conforti, A. Locatelli, C. De Angelis, A. Parini, G. Bellanca, and S. Trillo, "Self-pulsing instabilities in backward parametric wave mixing, J. Opt. Soc. Am. B **22**, 2178-2184 (2005).

[23] N.D. Sankey, D.F. Prelewitz, and T.G. Brown "All-optical switching in a nonlinear periodic-waveguide structure" Appl. Phys. Lett. **60**, 1427-1429 (1992).

[24] A. Yariv and P. Yeh, *Optical waves in crystals* (J. Wiley & Sons, 1984).

[25] T. P. Valkering and S. A. Van Gils, "Geometrical approach to stationary waves in a shallow grating", Opt. Quantum Electron. **35** 959-966 (2003).

[26] J. Danckaert, C. Foebelets, and I. Veretennicoff, "Combined DFB and Fabry-Perot structures with a phase-matching layer for optical bistable devices", Phys. Rev. **44**, 8214-8225 (1991).

[27] S. Dutta Gupta, *Nonlinear optics of stratified media*, Progress in Optics XXXVIII, E. Wolf ed. (Elsevier, Amsterdam, 1998).